Geoderma 470 (2026) 117848

Contents lists available at ScienceDirect

Geoderma

journal homepage: www.elsevier.com/locate/geoderma

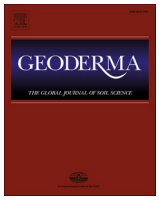

A semi-empirical model for soil moisture content retrieval based on the Kubelka-Munk model

Lihan Chen [a], Wei Xu [a], Xiaolei Chong [a], Kun Tan [b,c,d,*], Xue Wang [b,c,d], Zuoxia Yin [e], Jun Hu [f], Kai Xue [a], Hao Geng [a]

[a] Aviation Engineering School, Air Force Engineering University, Xi'an 710000, China
[b] School of GeoAI and Hindon STAI Institute, East China Normal University, Shanghai 200241, China
[c] Key Laboratory of Geographic Information Science (Ministry of Education), East China Normal University, Shanghai 200241, China
[d] Key Laboratory of Spatial-temporal Big Data Analysis and Application of Natural Resources in Megacities, Ministry of Natural Resources, East China Normal University, Shanghai 200241, China
[e] Jinan Real Estate Registration Center, Jinan 250000, China
[f] Air Defense and Antimissile School, Air Force Engineering University, Xi'an 710000, China

ARTICLE INFO

Handling Editor: H. Neely

Keywords:
Soil moisture content
Kubelka-Munk model
Reflectance
Remote sensing

ABSTRACT

Soil moisture is a critical factor influencing crop phenological development, climate patterns, and environmental changes. Accurate monitoring of soil moisture is therefore crucial for the natural ecological environment. The traditional methods of soil moisture monitoring are time-consuming and labor-intensive, so it is essential to establish a soil moisture retrieval model using remote sensing technology, meeting the needs for rapid monitoring and large-scale areas. Among the many methods, a radiative transfer model can explain the relationship between the optical properties of the soil media and soil moisture from the spectral mechanism. A semi-empirical radiative transfer model—the soil moisture Kubelka-Munk (SM-KM) model—is presented here to describe the relationship between soil moisture and soil spectra through the optical parameters, based on the Kubelka-Munk (KM) model. Four types of soil were utilized to validate the ability of the model, which closely simulate the reflectance of different soils in various moisture contents. Since the model requires soil moisture gradient data as boundary conditions, simplification of this model should be conducted in practical application. The soil moisture index (SMI_{KM}) was constructed with the SM-KM model, which enables the retrieval of soil moisture based solely on the spectral information. The index was validated using Sentinel-2 Multi-Spectral Instrument (MSI) data from Yitong County, Jilin province, China, where it obtained good results with R_C^2 of 0.640 and R_p^2 of 0.633. A soil moisture content map was also generated using the SMI_{KM} index. The proposed approach represents a convenient and rapid method for soil moisture estimation.

1. Introduction

Soil moisture, which is an important element of the terrestrial surface system, affects the energy balance and water cycle at regional to global scales (Patel et al., 2009; Badía et al., 2017; Kumar et al., 2018). As an indispensable component within the Earth's ecosystem, soil moisture engages in a sequence of hydrological cycle activities, encompassing surface runoff, groundwater replenishment, and vegetation absorption and transpiration, along with soil evaporation. Through altering surface reflectivity and heat capacity, and the conveyance of sensible and latent heat to the atmosphere, soil moisture assumes a pivotal role in climate change feedback. It serves as a key influencing factor in the exchange of water and material energy between soil, plants, and the atmosphere, constituting an essential substance for the growth and development of plants, profoundly impacting hydrological and biochemical processes within ecosystems (Heathman et al., 2012; Bogena et al, 2013; Ainiwaer et al., 2020). Accurate and timely monitoring of soil moisture is essential for agricultural production, water resource management, natural disaster warning, ecological environmental protection, climate change research, etc., thus supplying a scientific basis for achieving sustainable development and ecological health (Yang et al., 2012; Kang et al., 2016; Suyoung et al., 2017; Holzman et al., 2018). Traditional soil moisture

* Corresponding author at: School of GeoAI and Hindon STAI Institute, East China Normal University, Shanghai 200241, China.
E-mail address: tankuncu@gmail.com (K. Tan).

https://doi.org/10.1016/j.geoderma.2026.117848
Received 21 September 2025; Received in revised form 29 April 2026; Accepted 5 May 2026

measurement methods, such as the gravimetric drying-weighing method, resistance sensors, capacitance probes and time-domain reflectometry (TDR), are inherently point-based techniques. Their spatial coverage is severely limited by the density of monitoring networks, making it challenging to adequately capture the spatial heterogeneity of soil moisture and achieve continuous monitoring over large areas. While digital soil mapping and other spatial interpolation approaches can partially address this limitation, they still rely heavily on sparse in-situ measurements and often fail to capture fine-scale temporal dynamics. In contrast, remote sensing technology provides a non-destructive, spatially continuous and efficient alternative for large-scale soil moisture content retrieval. Remote sensing based soil moisture content retrieval methods can be broadly categorized into two main types: microwave remote sensing methods and optical remote sensing methods. Microwave remote sensing utilizes electromagnetic waves in the microwave frequency range (typically L-band) to penetrate the Earth's surface and measure the soil's dielectric properties, which are directly related to its volumetric water content. This approach allows for the direct sensing of the top few centimeters (0–5 cm)(Shen et al., 2021) of the soil layer. It is important to note that both microwave and optical remote sensing methods are inherently limited to retrieving near-surface soil moisture (typically the top 0–5 cm). This stands in contrast to in situ measurement techniques such as time-domain reflectometry (TDR) or capacitance probes, which can characterize soil moisture at deeper depths or across the entire root zone (0–70 cm) (Polak and Wallach, 2001). Notable satellite missions, such as the Advanced Microwave Scanning Radiometer for EOS (AMSR-E) (Yao et al., 2021) and the Soil Moisture and Ocean Salinity (SMOS) (Kerr et al., 2012) missions, have demonstrated the capability of microwave remote sensing in providing global-scale soil moisture information. However, limitations in the spatial resolution pose a challenge. These methods have high temporal resolution (1–3 days) and strong all-weather capability, yet their coarse spatial resolution (25–50 km) limits field-scale applications. In contrast, Sentinel-1 SAR delivers much higher spatial resolution (10 m) data, capturing fine-scale surface heterogeneity, though its signals are susceptible to interference from terrain undulations, vegetation coverage and surface roughness (Goyal et al., 1999; Adrian et al., 2021). On the other hand, optical methods (e.g., using Sentinel-2) estimate soil moisture by measuring surface reflectance in visible to shortwave infrared bands, typically offering high spatial resolution and rich spectral features for characterizing fine-scale spatial patterns. In summary, while microwave data enable robust, all-weather monitoring, visible/shortwave infrared data are superior for resolving detailed spatial distribution patterns of soil moisture.

In recent years, hyperspectral remote sensing, with its rich spectral information, has been widely utilized in soil property estimation (Chen et al., 2022; Tan et al., 2023). Statistical methods combined with hyperspectral remote sensing techniques have been widely used for soil moisture retrieval (Du et al., 2020), including partial least squares (PLS) (Morellos et al., 2016), support vector machine (SVM) (Araya-López et al., 2018), and artificial neural networks (ANNs) (Wang et al., 2018). Although these data-driven approaches can effectively model the relationship between soil reflectance and moisture content, their performance often relies heavily on sufficient calibration data and representative training samples. Furthermore, most such applications typically use spectral information alone, without incorporating important auxiliary factors such as soil texture, mineral composition, surface roughness, and vegetation cover, which may restrict their ability to provide physically consistent explanations for spectral variations caused by changes in soil moisture. Radiative transfer models describe the propagation and interaction of light with soil, considering the relationship between the soil optical properties and soil moisture, organic matter, metal oxides, etc. These models exhibit broad applicability, a robust theoretical foundation, and model parameters endowed with distinct physical significance. Jacquemoud et al. (1992) derived the SOILSPECT radiative transfer model, which is applicable to soil based on the Hapke model, and found that soil moisture content was negatively correlated with the single-scattered reflectance. Roosjen et al. (2015) studied the effects of soil moisture content on anisotropic reflectance with the Rahman-Pinty-Verstraete (RPV) model, and the results indicated that reflectance anisotropy contains more information on soil moisture content than spectral reflectance. Yang et al. (2011) found that soil moisture has a significant effect on soil bidirectional reflectance - characteristics and established the SWAP-Hapke model by improving the SOILSPECT model to retrieve soil moisture content. However, fully physical radiative transfer models involve complex mathematical solutions and require numerous difficult-to-measure soil parameters (single-scattering albedo and phase function) as prior inputs. They also rely on simplifying assumptions about soil surface roughness and particle size distribution, and their performance can degrade significantly when these assumptions are violated, which restricts their direct operational use.

In contrast, semi-empirical models strike a deliberate balance between physical consistency and practical feasibility. While they retain key physical constraints to avoid the poor generalization of purely empirical statistical models, they intentionally simplify complex radiative transfer processes and introduce empirical coefficients calibrated against local field data. This trade-off greatly reduces solution complexity and parameter demands, but it also means their accuracy and applicability are inherently tied to the representativeness of the calibration dataset, and they may not perform well across contrasting soil types, moisture ranges, or surface conditions. Semi-empirical models, while reinforcing the theoretical foundation, simultaneously avoid the issues of insufficient accuracy and difficult solutions associated with the physical modeling approaches. Lobell and Asner (2002) developed a simple moisture-reflectance model based on dry soil reflectance and the rate of change due to soil moisture. Zhang et al. (2020) proposed a novel soil moisture retrieval model based on the Hapke model and developed a new normalized difference soil moisture index to estimate soil moisture content. Sadeghi et al. (2015) presented a physical-based soil moisture retrieval model based on the Kubelka-Munk (KM) two-flux radiative transfer theory.

The Kubelka-Munk (KM) model, as a two-flux radiative transfer model considering only the upward and downward fluxes, provides a theoretical framework for linking soil composition to spectral reflectance, and has been applied in soil property estimation (Yuan et al., 2019; Ou et al., 2022; Wu et al., 2023). However, it often requires prior information that is difficult to determine, and lacks explicit equations to directly relate the fundamental optical parameters to soil moisture content, limiting its practical utility.

To address these gaps, this paper makes contributions that advance the application of KM theory in soil moisture retrieval: (i) A novel parameterization scheme: We propose a semi-empirical model (SM-KM) to explore the relationships between soil moisture content and soil optical parameters. (ii) A new physically-based index: Derived from the SM-KM model, a simplified soil moisture index (SMI_{KM}) is constructed. It is theoretically grounded, directly linked to the response of the soil optical parameters to moisture at two key wavelengths. (iii) Practical validation: We demonstrate the operational feasibility of this approach by generating a soil moisture content map using Sentinel-2 MSI data and the SMI_{KM} index.

2. Experimental data

2.1. Lobell and Asner soil spectra dataset

The laboratory spectra of four soils (Aridisol, Andisol, Mollisol, Entisol) with a series of soil moisture gradients were used in this study (Table 1). These soils were selected from diverse climatic and ecosystem settings, covering a wide range of bulk density, porosity, and organic carbon content (Lobell and Asner, 2002). The spectra at different soil moisture content gradients were determined by the use of an Analytical

Table 1
Details of the four soil types.

Soil type	Ecosystem type	Bulk density ($g \cdot cm^{-3}$)	Soil moisture content	
			Levels	Range
Aridisol	Arid shrubland	1.54	10	0–0.319
Andisol	Temperate coniferous forest	1.12	10	0–0.584
Mollisol	Temperate savanna	0.64	14	0–0.696
Entisol	Temperate shrubland	1.35	7	0–0.442

Spectral Devices (ASD) spectroradiometer under specific measurement conditions. The standard light source was directed at the plane from a zenith angle of 15°. Reflectance was calibrated using a white spectralon panel, and the soil spectra were collected approximately 4 cm above the plane. Soil samples were placed in blackened aluminum cans for the spectral measurements to avoid interference from background reflection. The spectra and water content under different moisture gradients were measured using the ASD spectroradiometer and mass measurements, respectively. The process was repeated by adding deionized water with a pipette until the soil reached saturation. Ultimately, soil spectra were obtained for the four types of soil under different moisture gradients.

Considering the correlation between the heights of adjacent spectra, these spectra were resampled at 10 nm intervals, in view of the correlation of adjacent bands, and then smoothed using the Savitzky-Golay smoothing method with a filtering window size of 9. The spectral curves of the four soil types are shown in Fig. 1.

From Fig. 1, it can be observed that the spectral shapes of the different soils are distinct. The spectra of the same soil under different moisture conditions exhibit similar shapes, showing approximately parallel trends. Soil moisture has a significant impact on the optical properties of the soil. In the visible range, there is a minimal change in the spectral curve, while in the shortwave infrared range, especially at the absorption peaks around 1400 nm and 1900 nm, variations occur with different moisture levels.

2.2. Yitong soil samples and imagery data

The study region is located in Yitong County, Jilin province, China. The terrain in this area is relatively gentle, with an average elevation of 305 m. The lowest elevation is 215 m, and the highest elevation is 430 m. The Yitong River runs through the whole study area from southeast to northwest. The annual average temperature is 5.5 °C, the annual average precipitation is 651.7 mm, and the annual average frost-free period is 138 days. The main soil types in the study area are dark brown soil (Haplic Cambisol, WRB), white pulpy soil (Albic Luvisol, WRB), meadow soil (Gleyic Cambisol, WRB), and black soil (Luvic Phaeozem, WRB). These soils represent distinct pedogenetic types with significant differences in organic matter content, particle size distribution, mineral composition, and pore structure. Notably, the black soil corresponds to the Mollisol used in the development of the Kubelka-Munk (KM) model, sharing similar high organic matter content and granular structure. Meanwhile, the inclusion of Cambisol, Luvisol, and Gleysol extends the validation scope beyond the original KM training dataset (which included Aridisol, Andisol, and Entisol), allowing a more comprehensive assessment of the model's generalization ability across different soil-forming environments.

Sixty-five soil points were sampled based on the grid sampling method from late April to early May 2019. The study area was divided using a grid system, with at least one sampling point established to each

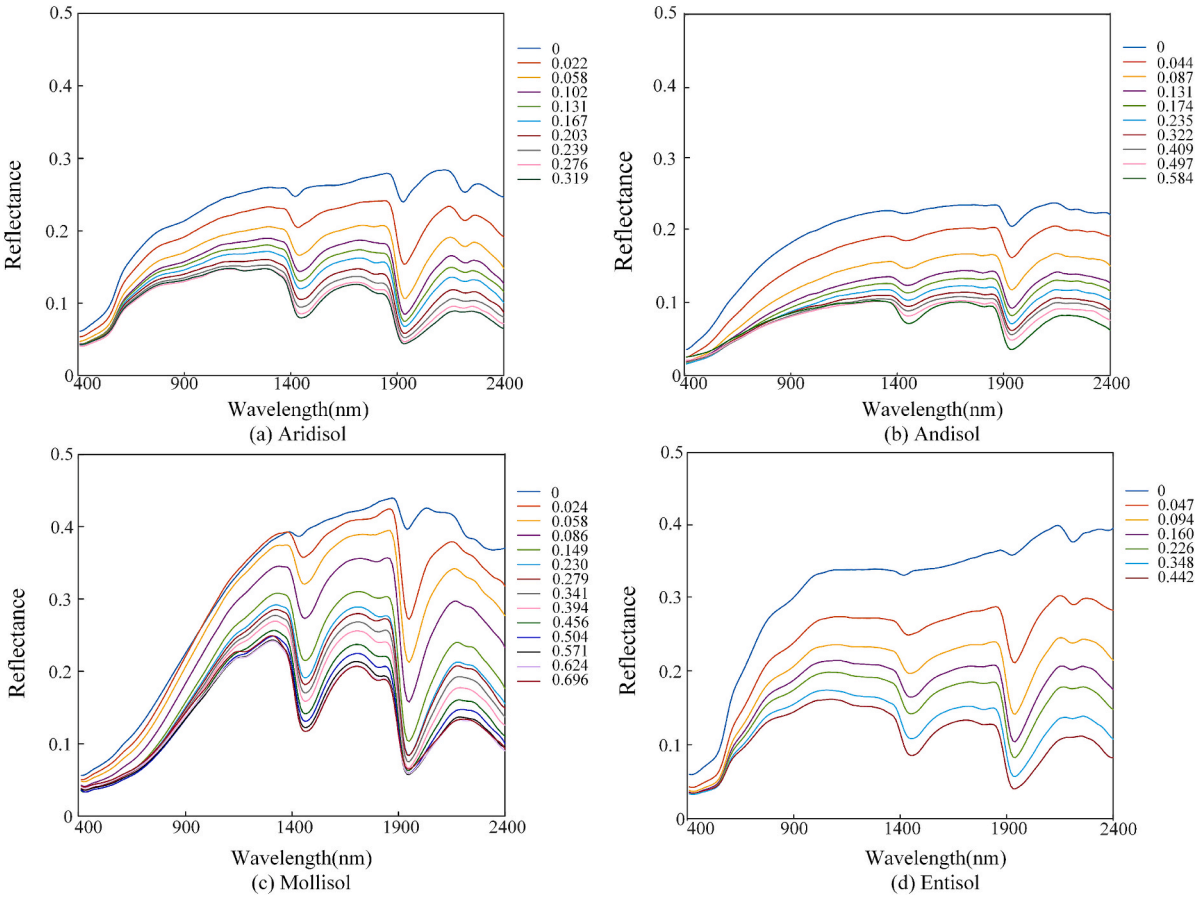

Fig. 1. The spectral curves of the four soil types at different soil moisture content gradients.

grid to ensure the spatial uniformity and representativeness. During the specific implementation, considering the feasibility of fieldwork, if the preset point located in an inaccessible area, the sampling position will be adjusted. Sampling is conducted in the top 0–5 cm of the soil layer. During this period, most farmlands in the study area had completed plowing, with the surface covered by freshly tilled soil. Therefore, the actual amount of crop residue present is relatively low, and its interference with spectral signals has been reduced.

Fig. 2 shows the study area and sampling point locations. In order to prevent the evaporation of moisture from affecting the measurement results, the soil samples were immediately packed into watertight light-blocking sealed bags and brought back to the laboratory. One part was used with an ML3X soil moisture meter to measure the volumetric moisture content ($cm^3.cm^{-3}$) of the soil. The statistics for the soil moisture contents of these samples are listed in Table 2.

Table 3 lists the main band information of the Sentinel-2 satellite. Sentinel-2 is a high-resolution multispectral imaging satellite developed by the European Space Agency (ESA), which carries a Multi-Spectral Instrument (MSI) sensor, providing images of vegetation, soil and water cover, inland waterways, and coastal areas. Sentinel-2 MSI data with 13 spectral bands, covering the VIS–NIR–SWIR electromagnetic frequency domains, were acquired from the ESA Sentinel Scientific Data Hub on 4 May 2019. The field soil sampling was conducted from late April to early May 2019, and the Sentinel-2 satellite image was acquired exactly within the sampling period. This temporal alignment ensured minimal changes in soil moisture conditions due to precipitation, evaporation, and vegetation phenology. No extreme weather events occurred during this period, and the image was captured under clear-sky conditions with no cloud or shadow contamination, guaranteeing both the temporal consistency and high data quality of remote sensing observations.

Original Level 1C data were preprocessed using the SNAP data processing software and Sen2Cor toolkit to perform atmospheric, topographic and cirrus correction, and then generate the Level 2A surface reflectance product. The 60-meter resolution bands (Band 1, Band 9, and Band 10) were removed. The image was resampled to 10-m resolution with the cubic convolution interpolation method. Following the above processing, a 10-band, 10-meter resolution Sentinel-2 multispectral image was ultimately generated.

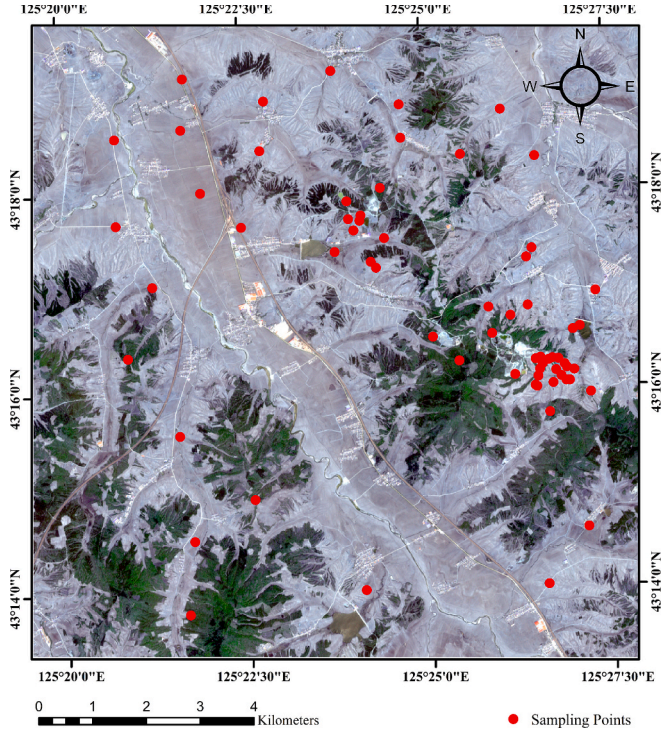

Fig. 2. The locations of the sampling sites in the study region.

Table 2
Basic statistics of the soil moisture content in the study region.

	Min (%)	Max (%)	Mean (%)	Std.	CV.
Soil moisture content	0.53	26.1	6.21	0.05	0.81

Table 3
Spectral bands for the Sentinel-2 sensor.

Band number	Central Wavelength (nm)	Bandwidth (nm)	Spatial Resolution (m)
Band 1	442.2	21	60
Band 2	492.1	66	10
Band 3	559.0	36	10
Band 4	664.9	31	10
Band 5	703.8	16	20
Band 6	739.1	15	20
Band 7	779.7	20	20
Band 8	832.9	106	10
Band 8A	864.0	22	20
Band 9	943.2	21	60
Band 10	1376.9	30	60
Band 11	1610.4	94	20
Band 12	2185.7	185	20

3. Method

3.1. SM-KM semi-empirical model

Kubelka-Munk (K-M) theory (Kubelka and Munk, 1931) is a theory proposed by Paul Kubelka and Franz Munk in 1931 to describe the absorption and scattering of light in a medium, considering the upper and lower fluxes of light perpendicular to the interface (Fig. 3).

The light flux in the lower direction and upper direction are defined as I are J, respectively, and the energy balance differential equation of the double flux is as follows:

$$\frac{dI(\lambda,z)}{dz} = -(K+S)I(\lambda,z)+SJ(\lambda,z) \quad (1)$$

$$\frac{dJ(\lambda,z)}{dz} = (K+S)J(\lambda,z)-SI(\lambda,z) \quad (2)$$

where z is the thickness of the soil cross through the light, λ is the wavelength, and K and S are the absorption and scattering coefficients of soil, respectively(Vargas and A, 1997; Wu et al., 2023). Equation (1) and Equation (2) can be solved by the following equation:

$$I(\lambda,z) = I_0(\lambda)[\mu(1-\beta)\exp(\alpha z)+\nu(1+\beta)\exp(-\alpha z)] \quad (3)$$

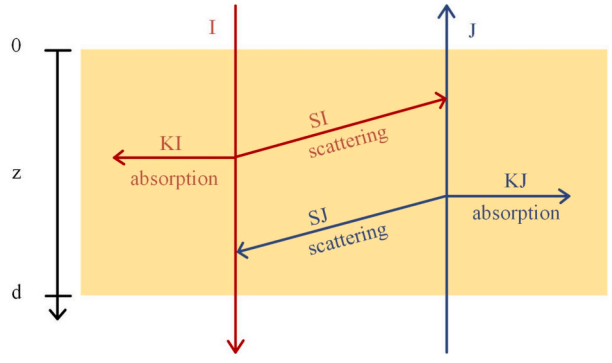

Fig. 3. Schematic representation of the KM model.

$$J(\lambda, z) = I_0(\lambda)[\mu(1+\beta)\exp(\alpha z) + \nu(1-\beta)\exp(-\alpha z)] \quad (4)$$

where $\alpha \equiv \sqrt{K(K+2S)}$ and $\beta \equiv \sqrt{K/(K+2S)}$.$I_0(\lambda)$ represents the intensity of light on the surface of the soil, and μ and ν depend on the boundary conditions. When light passes through the soil layer,$z = d$. μ and ν are calculated by the following equation:

$$\mu = \frac{-(1-\beta)\exp(-\alpha d)}{(1+\beta)^2\exp(\alpha d) - (1-\beta)^2\exp(-\alpha d)} \quad (5)$$

$$\nu = \frac{(1-\beta)\exp(\alpha d)}{(1+\beta)^2\exp(\alpha d) - (1-\beta)^2\exp(-\alpha d)} \quad (6)$$

The soil reflectance R and transmittance T can be defined as:

$$R = \frac{J(z=0)}{I_0(\lambda)} \quad (7)$$

$$T = \frac{J(z=d)}{I_0(\lambda)} \quad (8)$$

The analytical solution for the reflectance R and transmittance T can be given as follows:

$$R = \frac{(1-\beta)^2[\exp(\alpha d) - \exp(-\alpha d)]}{(1+\beta)^2\exp(\alpha d) - (1-\beta)^2\exp(-\alpha d)} \quad (9)$$

$$T = \frac{4\beta}{(1+\beta)^2\exp(\alpha d) - (1-\beta)^2\exp(-\alpha d)} \quad (10)$$

With the increase of soil thickness d, the transmittance tends to zero and the reflectance reaches a stable state, which is called the infinite reflectance R_∞. Further increases in the thickness of the sample do not affect the measured signal, and thus Equation (9) can be simplified as (Ciani et al., 2005):

$$R_\infty = \frac{1-\beta}{1+\beta} = 1 + \frac{K}{S} - \sqrt{\left(\frac{K}{S}\right)^2 + 2\frac{K}{S}} \quad (11)$$

After Transform by $r = \frac{K}{S}$,r can be calculated as:

$$r = \frac{K}{S} = \frac{(1-R_\infty)^2}{2R_\infty} \quad (12)$$

The absorption coefficient and scattering coefficient of the mixture in the KM model are generally considered to be the proportionally weighted sum of the absorption coefficient and scattering coefficient of each substance. Based on this assumption, considering the influence of soil moisture content, the absorption coefficient K and scattering coefficient S of the soil are expressed as:

$$K = K_d + K_w\theta \quad (13)$$

$$S = S_d + S_w\theta \quad (14)$$

where K_d and K_w denote the absorption coefficients of dry soil and moist soil, respectively; S_d and S_w represent the scattering coefficients of dry soil and moist soil, respectively; and θ is the soil moisture content.

This linear parameterization greatly reduces model complexity, avoids the need for difficult-to-measure optical parameters, and enables practical estimation of soil moisture from observed reflectance. It should be noted, however, that this represents a simplifying assumption that may not fully capture the complex interactions between soil particles and water films, as well as the influences of soil texture, organic matter content, and pore structure on optical properties. Furthermore, it does not explicitly account for the differential effects of water distribution within pore spaces on soil absorption and scattering characteristics. Despite these limitations, this linear approximation is widely adopted in soil radiative transfer modeling for its simplicity and computational efficiency.

With the increase of θ, the absorption and scattering coefficients of soil with saturated water capacity are as follows:

$$K_s = K_d + K_w\theta_s \quad (15)$$

$$S_s = S_d + S_w\theta_s \quad (16)$$

where θ_S indicates the saturated moisture content.

Combining Equations (11) to (16) yields:

$$r = \frac{K}{S} = \frac{K_s - K_w(\theta_s - \theta)}{S_s - S_w(\theta_s - \theta)} \quad (17)$$

With $r_s = \frac{K_s}{S_s}$, $a_1 = \frac{K_w}{S_s}$, and $a_2 = \frac{S_w}{S_s}$,r can be calculated as:

$$r = \frac{r_s - a_1(\theta_s - \theta)}{1 - a_2(\theta_s - \theta)} \quad (18)$$

Soil moisture content θ can be calculated as:

$$\theta = \theta_s - \frac{r - r_s}{ra_2 - a_1} \quad (19)$$

3.2. Soil moisture index based on the KM model: SMI_{KM}

The SM-KM model can effectively retrieve soil moisture through the interaction mechanism between soil moisture and spectra. However, since the optical properties of soil change with its composition and physicochemical properties, gradient data of each sample are required for the SM-KM model as the boundary conditions for the model establishment, to solve the model parameters and achieve soil moisture retrieval. To address this issue, it is necessary to simplify the model and reduce the calibration difficulty without compromising its physical significance. In the strong absorption bands of water, the scattering effect of soil moisture is very weak, compared to the scattering effect of soil particles, and can be neglected. This simplification is justified under two conditions: (1) the selected spectral bands are located in strong water absorption regions; and (2) soil moisture content is not excessively high (not approaching saturation). When soil moisture becomes very high, continuous water films may form on soil particle surfaces, and the scattering contribution of water is no longer negligible, making the simplified linear relationship invalid. Therefore, the scattering effect of soil moisture can be neglected, a_2 can be considered as 0, and Equation (19) can be simplified as:

$$\theta = \theta_s + \frac{r - r_s}{a_1} \quad (20)$$

It can be observed from Equation (20) that there is a linear relationship between θ and r, and θ can be calculated through this linear relationship. The strong water vapor absorption bands are at 1400 nm and 1900 nm, which have a negative influence on soil moisture content retrieval. It is therefore necessary to select suitable bands to retrieve the soil moisture content. The shortwave infrared bands are more sensitive to water. Consistent with the physical requirement of the simplified KM model, we select the 1610 nm and 2200 nm bands. Both bands fall within strong water absorption regions (Viscarra Rossel and Behrens, 2010; Knadel et al., 2013). Hence, the band selection is primarily constrained by the KM model's validity conditions, while the empirical studies serve as supporting evidence for the bands' sensitivity to soil moisture. In order to improve the accuracy of the retrieval and reduce the influence of instrument error, multi-band combination can be utilized for soil moisture content retrieval. Consequently, considering the correlation between soil moisture and r of the two bands, a soil moisture index SMI_{KM} can be constructed to estimate soil moisture content. We adopt the normalized difference form to minimize the influence of soil type variations and measurement noise. SMI_{KM} can be calculated as:

$$SMI_{KM} = \frac{r_{1610} - r_{2200}}{r_{1610}} \quad (21)$$

where r_{1610} and r_{2200} represent the value of r at 1610 nm and 2200 nm.

To further verify the reliability and advancement of the constructed soil moisture index, we compare it with two typical soil moisture indices from the literature that are also based on shortwave infrared bands: the shortwave infrared transformed reflectance (STR) and the normalized shortwave-infrared difference bare soil moisture index (NSDSI1). Both indices were selected because they: (1) are both based on shortwave infrared bands sensitive to soil moisture variations; (2) rely on spectral bands compatible with Sentinel-2 data and cover the main forms of existing empirical soil moisture indices; and (3) represent different mathematical formulations (a transformed reflectance for STR, and a normalized difference for NSDSI1). Details of these two indices are provided in Table 4.

3.3. Bare soil extraction using support vector machine classification method

Support Vector Machine (SVM) (Cortes and Vapnik, 1995) is a supervised classification algorithm based on statistical learning theory. Its core idea is to find an optimal hyperplane in the feature space, which can clearly separate different classes of samples while maximizing the distance between the nearest samples of the two classes to the plane, thereby ensuring the generalization ability of the classifier. When the samples are linearly inseparable in the original space, SVM maps the data to a higher-dimensional feature space through a kernel function, enabling linear separation in the high-dimensional space. This method performs well in problems of small samples, high dimensions, and nonlinear pattern recognition, and is widely applied in fields such as remote sensing image classification and target recognition.

In this study, the soil moisture retrieval model is developed based on the bare soil spectra, as vegetation cover would alter the reflectance. Therefore, it is necessary to extract bare soil area before applying the soil moisture retrieval. To this end, we apply SVM to classify the land cover of the study area. In the imagery of study area, regions of interest (ROIs) were uniformly annotated for five typical land cover types, bare soil, vegetation, water bodies, buildings, and roads, to form the training dataset. Supervised classification was performed using SVM, and the bare soil areas of the entire image were extracted. Subsequently, the soil moisture content is estimated only for the extracted bare soil area.

3.4. Sample set portioning based on the joint x-y distance

The sample set portioning based on joint x-y distance (SPXY) method, which is based on the Kennard-Stone (KS) method, takes into account the spectral information (x) and soil physicochemical properties (y) when dividing the data set (Galvao et al., 2005). The KS method first selects the samples with the largest spectral difference, and selects a sufficient number of samples by calculating the maximum Euclidean distance between the samples to be selected and the samples that have been selected. In contrast, the SPXY method takes into account the Euclidean distance on the x and y variables when calculating the distance between samples. The distance calculation equations are as follows:

$$d_x(p,q) = \sqrt{\sum_{j=1}^{J}\left[x_p(j) - x_q(j)\right]^2}; p,q \in [1,N] \tag{22}$$

Table 4
Typical soil moisture indices.

Soil moisture index	Equation	Reference
STR	$(1 - B_{2185})^2/2B_{2185}$	Sadeghi et al. (Sadeghi et al. 2017)
NSDSI1	$(B_{1694} - B_{2230})/B_{1694}$	Yue et al.(Yue et al. 2019)

$$d_y(p,q) = \sqrt{(y_p - y_q)^2} = \left|y_p - y_q\right|; p,q \in [1,N] \tag{23}$$

$$d_{xy}(p,q) = \frac{d_x(p,q)}{\max d_x(p,q)} + \frac{d_y(p,q)}{\max d_y(p,q)}; p,q \in [1,N] \tag{24}$$

where J represents the band in the spectrum. $x_p(j)$ and $x_q(j)$ represent the reflectance of p and q in band J, respectively, and N is the total number of samples. $d_x(p,q)$ and $d_{xy}(p,q)$ represent the Euclidean distance between two samples in the spectral feature space and soil moisture content, respectively.

Because the model can take into account the characteristics of the spectra and soil moisture content, the prediction accuracy of the established model can be significantly improved.

In order to explore the retrieval ability of SMI_{KM}, the surface reflectance of 65 field samples was extracted from the Sentinel-2 MSI data. The data set was divided using the SPXY method, with 43 samples for calibration and 22 samples for validation. The relatively small number of field samples and the limited size of the validation set are constraints of this study, which may limit the comprehensive evaluation of the model's generalization ability. However, the SPXY method was specifically adopted to maximize the representativeness of both subsets under the existing sample conditions.

3.5. Parameter optimization using genetic algorithm

The genetic algorithm was employed to optimize the four parameters of the SM-KM model: r_s, a_1, a_2 and θ_S. Genetic algorithm performs efficient parallel global searches within complex multidimensional parameter spaces by simulating core mechanisms of biological evolution-selection, crossover, and mutation. It excels at tackling complex optimization problems with discontinuous or highly nonlinear characteristics, effectively avoiding the pitfalls of traditional gradient-based methods that often get stuck in local optima. This algorithm finds extensive application in optimizing soil moisture inversion algorithm (Kara et al., 2024; Wang et al., 2024). Given the nonlinear nature of the SM-KM model and the potential for multiple local minima in its parameter space, the genetic algorithm is particularly suitable for this parameter optimization.

It is utilized as a function optimization algorithm, and the mean square error (MSE) is used as a cost function to measure the difference between the measured and simulated reflectance values, to determine the performance of the optimization. The MSE is defined as follows:

$$MSE(r_s, a_1, a_2, \theta_s) = \frac{1}{N}\sum_{m=1}^{N}\left[R_{mea}(\lambda) - R_{sim}(\lambda)\right]^2 \tag{25}$$

where $R_{mea}(\lambda)$ is the measured reflectance, and $R_{sim}(\lambda)$ is the simulated reflectance at the wavelength of λ. The genetic algorithm finds the equation parameters with the lowest cost function, so that the soil reflectance simulated by the model is as close as possible to the measured reflectance at different soil moisture contents.

3.6. Model evaluation method

Two indicators are employed to evaluate the model accuracy: the root-mean-square error (RMSE) and the coefficient of determination (R^2). Each indicator is calculated as follows:

$$RMSE = \sqrt{\frac{\sum_{i=1}^{N}(mea_i - pred_i)^2}{N}} \tag{26}$$

$$R^2 = 1 - \frac{\sum_{i=1}^{N}(mea_i - pred_i)^2}{\sum_{i=1}^{N}(mea_i - \overline{mea})^2} \tag{27}$$

where *mea* denotes the measured value, and *pred* denotes the predicted value. R_C^2 and $RMSE_C$ represent the calibration data set evaluation, and R_P^2 and $RMSE_P$ express the prediction data set evaluation.

3.7. Uncertainty evaluation using prediction interval width (PIW)

To quantitatively evaluate the uncertainty of the soil moisture retrieval results, prediction interval width (PIW) metric (Schmidinger and Heuvelink, 2023) which measures the sharpness of probabilistic predictions was adopted. Since this study focuses on a point prediction model, we used the residual quantile method to construct uniform prediction intervals (PIs), which assumes homoscedasticity of model errors. The prediction errors were calculated for all validation samples. Then, the bounds of the prediction intervals from the empirical distribution of these errors were derived. PIW indicates the width of a certain $\tau \times 100$ per cent PI, for any value of τ between 0 and 1:

$$\mathrm{PIW}(\tau) = \frac{1}{n}\sum_{i=1}^{n}(u_i - l_i) \tag{28}$$

where l_i is the lower bounding quantile and u_i the upper bounding quantile that together define a $\tau \times 100$ per cent PI. Usually, central PIs are of interest, meaning that the probability mass below l_i and above - u_i are equal. Therefore, l_i and u_i are determined by the chosen τ value:

$$l_i = q^i_{(1-\tau)/2} \tag{29}$$

$$u_i = q^i_{(1+\tau)/2} \tag{30}$$

where $q^i_{(1-\tau)/2}$ and $u_i = q^i_{(1+\tau)/2}$ are the $(1-\tau)/2$ and $(1+\tau)/2$ quantiles of the predictive distribution of y_i. Lower PIW values indicate higher prediction sharpness and lower retrieval uncertainty.

4. Results

4.1. SM-KM semi-empirical model

The model parameters were calculated with an interval of 10 nm in the range of 400–2400 nm. The MSE values with genetic algorithm between the measured reflectance and the simulated reflectance of the four soils in the whole wavelength are listed in Table 5.

It can be seen that the MSE is generally lower than 7×10^{-5}, indicating that the proposed SM-KM model has an excellent performance and can accurately simulate the reflectance of different soils in various moisture contents. The calculated optimal values are displayed in Fig. 4, which reflects the variation curves of the four unknown parameters for the four samples.

It is clear that parameters r_s and a_1 decrease from 400 nm and gradually become flat. There are distinct absorption peaks around 1400 nm and 1900 nm, and an absorption valley at 2200 nm. Water has strong absorption regions near 1400 nm and 1900 nm caused by the overtones and fundamentals of the vibration frequencies of H_2O (Knadel et al., 2013). The absorption at 2200 nm results from the O–H stretch combination vibration absorption (Viscarra Rossel and Behrens, 2010). The two parameters of θ_S and a_2 are small and vary insignificantly. The saturated moisture content of the soil is only related to the soil properties and is independent of the wavelength, as the θ_S variations are small. Due to the weak scattering ability and strong absorption ability of the water in the soil, the scattering effect can be neglected. Therefore, a_2 is very small and negligible.

Table 5
The MSE values between the measured reflectance and the simulated reflectance of the four soil types.

Soil type	MSE	Soil Type	MSE
Aridisol	7.92×10^{-6}	Andisol	1.66×10^{-5}
Mollisol	6.23×10^{-5}	Entisol	8.36×10^{-6}

In practical applications, it is necessary to obtain soil moisture gradient data for each sample as the boundary conditions for model calibration, and the calculation process is relatively complicated. In order to solve this problem, it is necessary to simplify the model and reduce the calibration difficulty of the model without destroying the physical meaning. Equation (21) is a simplification of the SM-KM model, in which the volumetric moisture content can be expressed as a linear function of r. As an illustration, Fig. 5 shows the linear fitting results between soil moisture content and r_{1610}, as well as the linear fitting results between soil moisture content and r_{2200} of the four soils, which verifies the applicability of Equation (21).

4.2. Performance evaluation of SMI_{KM}

SVM was used to extract the bare soil of the study area. A bare soil image of the study area is shown in Fig. 6.

Table 6 lists the estimation results obtained using the three indices. Compared to STR and NSDSI1, SMI_{KM} shows relatively better performance, with higher R^2 values. The R^2 values of SMI_{KM} in the calibration dataset and validation dataset are more than 0.6. Fig. 7 shows the scatter diagrams of soil moisture content estimation with the three soil moisture indices. The points estimated by SMI_{KM} tend to cluster somewhat closer to the 1:1 line than those of STR and NSDSI1, suggesting an improved estimation. The distribution of the points estimated by STR and NSDSI1 is more discrete.

In addition to the conventional accuracy indicators, we calculated PIW of each soil moisture index at a 90% confidence level. This indicator directly measures the uncertainty of the prediction. PIW of the prediction set calculated with three soil moisture index is shown in Table 7.

It is clearly that SMI_{KM} has lowest PIW values. Lower PIW values imply lower uncertainty. With the same level of confidence, SMI_{KM} can provide more accurate and less uncertain soil moisture predictions. Fig. 8 shows the estimation map for soil moisture content.

The trends of the soil moisture estimation maps generated by the three methods are in good agreement. This consistency supports the rationality and plausibility of the SMI_{KM} index. More importantly, this spatial coherence provides supporting evidence for the physical rationality of the core parameterization scheme within the SM-KM radiative transfer model. It demonstrates that the model effectively bridges the optical parameters described by Kubelka-Munk theory and the macroscopic soil moisture patterns. It provides area geographic-scale evidence that a physically constructed index can reliably capture the soil moisture signal in the study area.

5. Conclusion

In this paper, a semi-empirical radiative transfer model-SM-KM model-has been proposed. Its primary innovation is a novel parameterization scheme within the KM theory, describing the physical relationship between soil spectral reflectance and moisture content through optical parameters. Experimental results demonstrate that the SM-KM model effectively simulates spectral variations in different soil types under varying moisture conditions.

To overcome the limitations of the moisture gradient boundary conditions required for the SM-KM model in practical applications, this study further simplified it into a linear form, thereby deriving a soil moisture index (SMI_{KM}) that can be directly calculated based on spectral information. A notable improvement of this index is its derivation from a physical model, which helps avoid some of the regional limitations often associated with purely empirical indices. In an empirical study conducted in Yitong County, Jilin Province, China, using Sentinel-2 MSI data for validation, the SMI_{KM} index demonstrated stable accuracy with R_C^2 of 0.640 and R_p^2 of 0.633. Compared with the two soil moisture

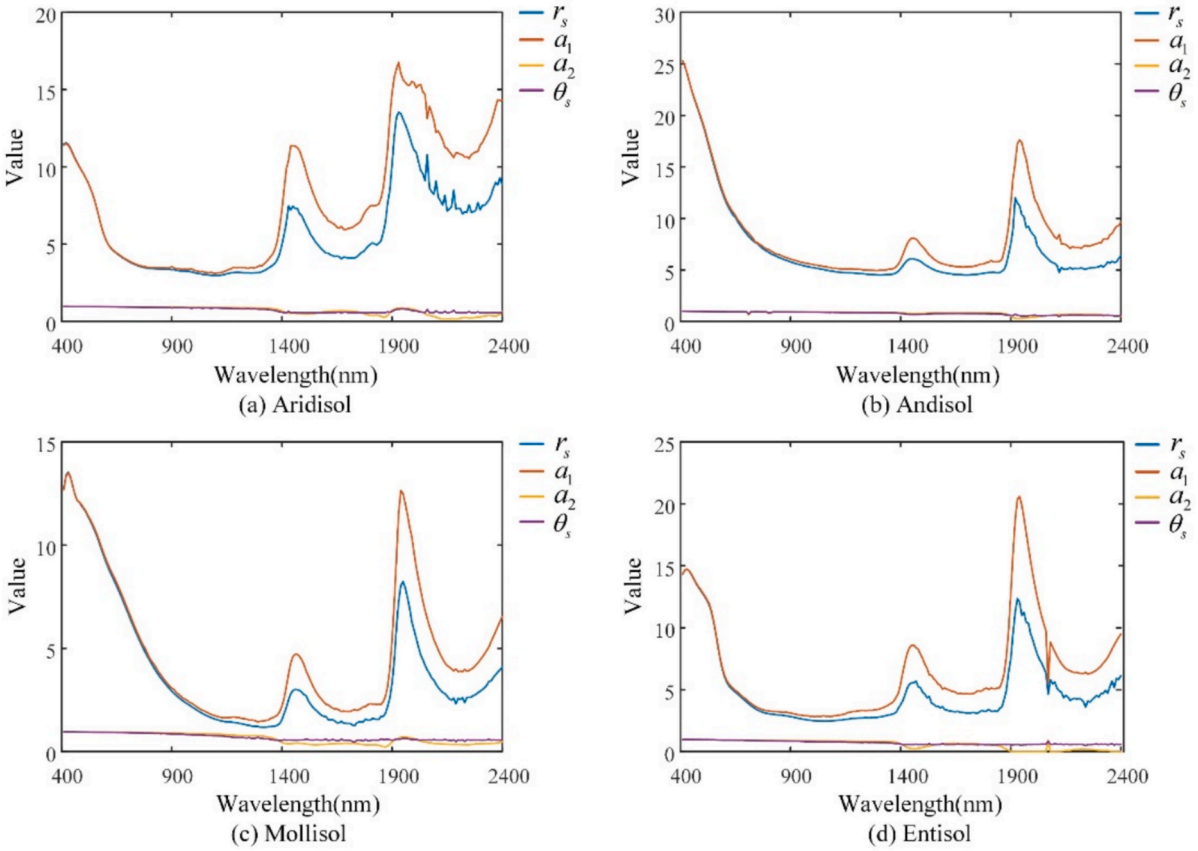

Fig. 4. Model parameters of the four soils.

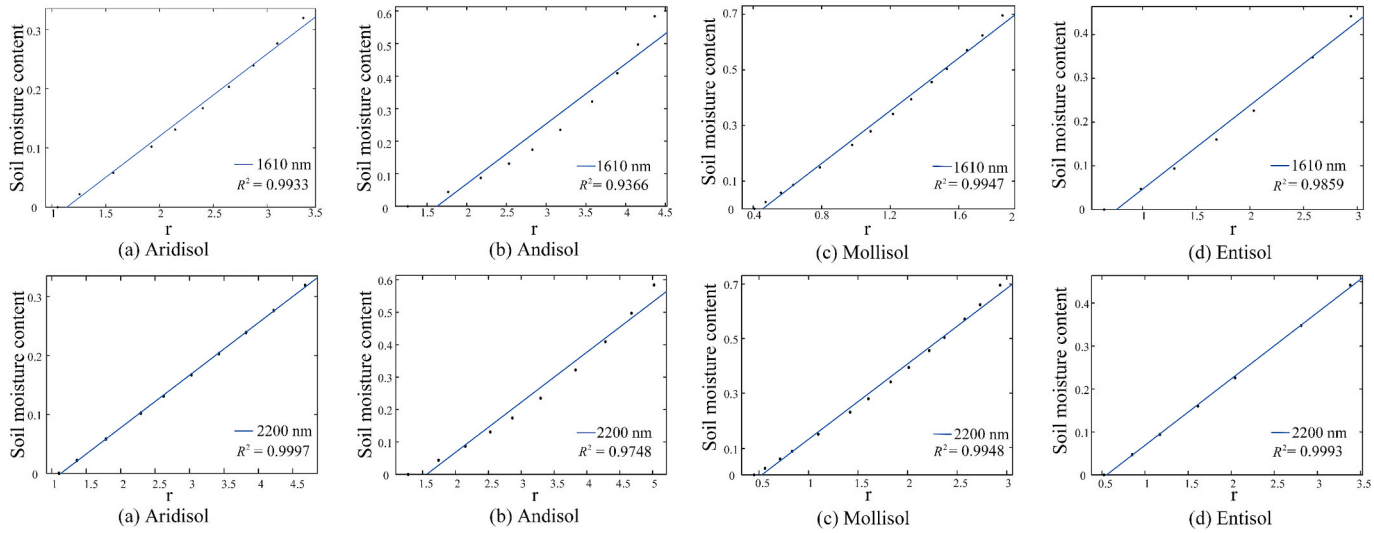

Fig. 5. Linear fitting results between soil moisture content and r_{1610}, as well as the linear fitting results between soil moisture content and r_{2200} of the four soils.

indices, SMI_{KM} showed competitive or improved performance for regional soil moisture estimation. To date, only a limited number of studies have used physical models to develop soil moisture indices. Compared with conventional empirical moisture indices, the SMI_{KM} index has clear physical significance, which provides advantages in interpretability and robustness. Furthermore, this method enables large-scale soil moisture estimation without requiring complex localized modeling processes.

The SMI_{KM} method proposed in this paper enables rapid and convenient estimation of soil moisture while preserving its physical basis, offering a promising practical tool for applications such as regional agricultural optimization, water resource management, and soil degradation monitoring. Additionally, the SMI_{KM} index can serve as a spectral correction method to isolate soil moisture effects, thereby enhancing the accuracy of remote sensing estimates for other critical soil parameters like organic matter and heavy metals.

We acknowledge that the model's universality still requires further validation across different geographical regions and soil conditions.

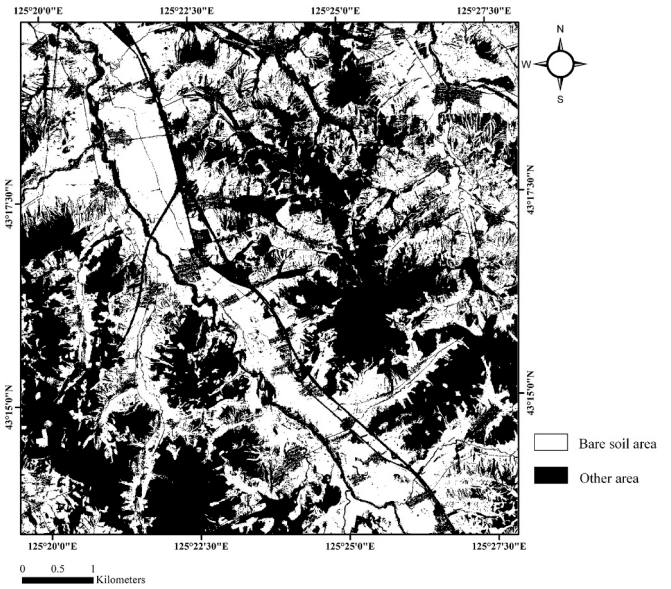

Fig. 6. Bare soil image of the study area.

Table 6
Estimation results between soil moisture content and soil moisture indices with Sentinel-2 data.

Index	R_C^2	$RMSE_C$	R_p^2	$RMSE_P$
STR	0.559	0.023	0.545	0.038
NSDSI1	0.586	0.024	0.583	0.036
SMI_{KM}	0.640	0.021	0.633	0.033

Note:R_C^2 and $RMSE_C$ represent the calibration data set evaluation, and R_P^2 and $RMSE_P$ express the prediction data set evaluation.

Furthermore, optical remote sensing data itself remains susceptible to weather conditions and sensor performance limitations. Therefore, subsequent research will focus on deepening the physical mechanism of the model and expanding its application capabilities. Specifically, future work will extract pure bare soil spectra through techniques such as spectral unmixing to optimize the model's robustness, and explore the application of SMI_{KM} to time-series analysis of satellites like Sentinel-2 for dynamic monitoring of soil moisture changes. To systematically enhance the reliability of the model in complex scenarios, we will quantitatively analyze the influences of key physical factors such as surface roughness, pore structure, and observation geometry, and investigating synergistic inversion schemes combining optical SMI_{KM} indices with radar data from satellites such as Sentinel-1 to achieve all-weather, more precise operational soil moisture monitoring. We fully recognize the importance of spatial cross-validation in large-scale applications and will strictly adopt this method in subsequent work to objectively evaluate the regional generalization ability of the model.

CRediT authorship contribution statement

Lihan Chen: Writing – original draft, Methodology, Data curation, Conceptualization. **Wei Xu:** Writing – review & editing, Formal analysis. **Xiaolei Chong:** Writing – review & editing, Formal analysis. **Kun Tan:** Writing – review & editing, Resources, Methodology. **Xue Wang:** Writing – review & editing, Project administration. **Zuoxia Yin:** Supervision. **Jun Hu:** Validation, Investigation. **Kai Xue:** Validation. **Hao Geng:** Visualization.

Declaration of competing interest

The authors declare that they have no known competing financial interests or personal relationships that could have appeared to influence

Table 7
PIW of STR, NSDSI1 and SMI_{KM}.

PIW	STR	NSDSI1	SMI_{KM}
Value	0.1116	0.1048	0.0956

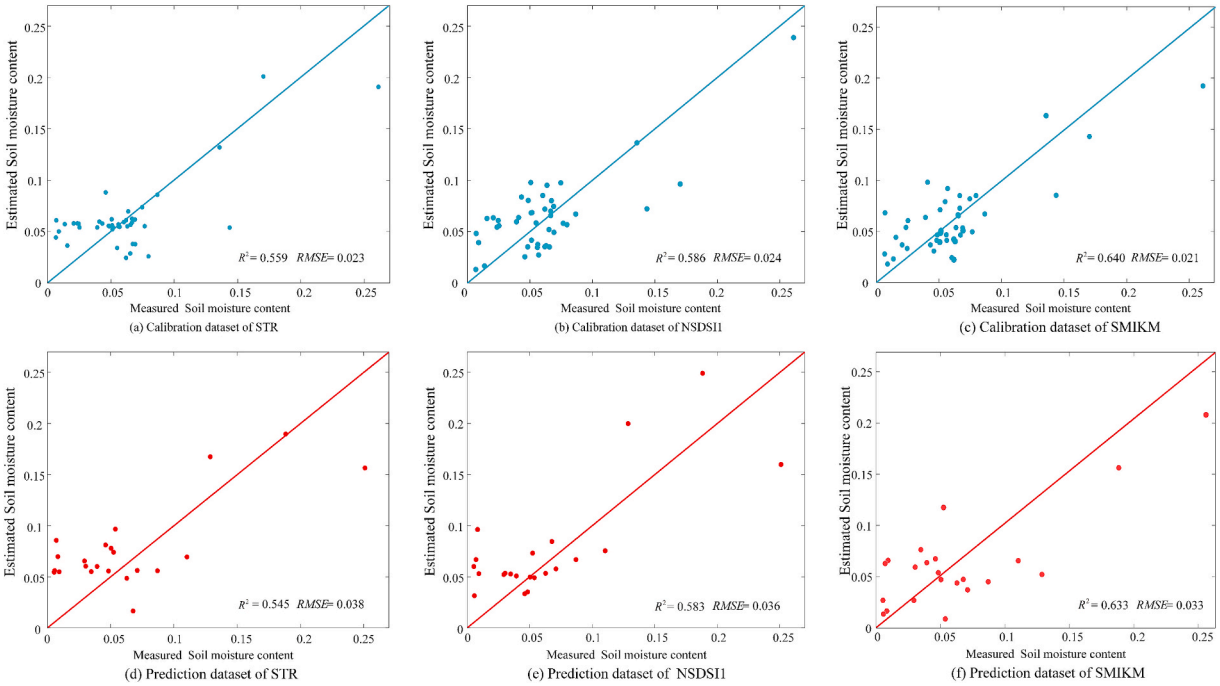

Fig. 7. Scatter diagrams of soil moisture content estimation. (a) Calibration dataset with STR, (b) calibration dataset with NSDSI1, (c) calibration dataset with SMI_{KM}, (d) prediction dataset with STR, (e) prediction dataset with NSDSI1, (f) prediction dataset with SMI_{KM}.

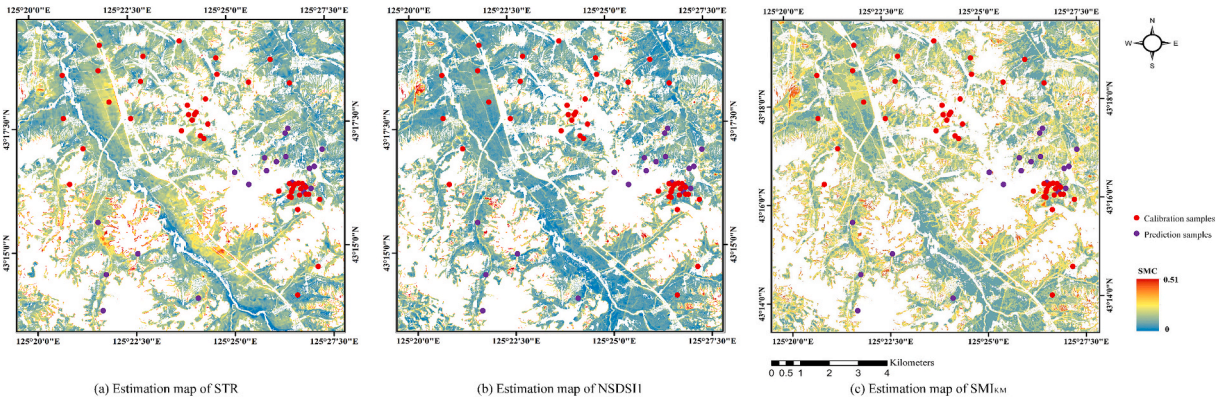

(a) Estimation map of STR (b) Estimation map of NSDSI1 (c) Estimation map of SMI_{KM}

Fig. 8. Estimation maps for soil moisture content. (a) Estimation map of STR, (b) estimation map of NSDSI1, (c) estimation map of SMI_{KM}.

the work reported in this paper.

Acknowledgment

This work was jointly supported by the National Natural Science Foundation of China (grant no. 42171335), the Shanghai Municipal Science and Technology Major Project (grant no. 22511102800), the National Civil Aerospace Project of China (grant no. D040102), the International Research Center of Big Data for Sustainable Development Goals (CBAS2022GSP07) and the Natural Science Basic Research Program of Shaanxi (grant no. 2023-JC-QN-0720).

Data availability

Data will be made available on request.

References

Adrian, J., Sagan, V., Maimaitijiang, M., 2021. Sentinel SAR-optical fusion for crop type mapping using deep learning and Google Earth Engine. ISPRS J. Photogramm. Remote Sens. 175, 215–235.
Ainiwaer, M., Ding, J., Kasim, N., Wang, J., Wang, J., 2020. Regional scale soil moisture content estimation based on multi-source remote sensing parameters. Int. J. Remote Sens. 41 (9), 3346–3367.
Araya-López, R.A., Lopatin, J., Fassnacht, F.E., Hernández, H.J., 2018. Monitoring Andean high altitude wetlands in central Chile with seasonal optical data: A comparison between Worldview-2 and Sentinel-2 imagery. ISPRS J. Photogramm. Remote Sens. 145, 213–224.
Badía, D., López-García, S., Martí, C., Ortíz-Perpiñá, O., Girona-García, A., Casanova-Gascón, J., 2017. Burn effects on soil properties associated to heat transfer under contrasting moisture content. Sci. Total Environ. 601–602, 1119–1128.
Bogena, H.R., Huisman, J.A., Baatz, R., Franssen, H.J.H., Vereecken, H., 2013. Accuracy of the cosmic-ray soil water content probe in humid forest ecosystems: the worst case scenario. Water Resour. Res. 49 (9), 5778–5791.
Chen, L., Lai, J., Tan, K., Wang, X., Chen, Y., Ding, J., 2022. Development of a soil heavy metal estimation method based on a spectral index: combining fractional-order derivative pretreatment and the absorption mechanism. Sci. Total Environ. 813, 1–12.
Ciani, A., Goss, K.U., Schwarzenbach, R.P., 2005. Light penetration in soil and particulate minerals. Eur. J. Soil Sci. 56 (5), 561–574.
Cortes, C., Vapnik, V., 1995. Support-vector networks. Mach. Learn. 20 (3), 273–297.
Du, P., Bai, X., Tan, K., Xue, Z., Liu, W., 2020. Advances of four machine learning methods for spatial data handling: a review. J. Geovisualization Spatial Anal. 4 (13).
Galvao, R.K.H., Araujo, M.C.U., Jose, G.E., Pontes, M.J.C., Silva, E.C., Saldanha, T.C.B., 2005. A method for calibration and validation subset partitioning. Talanta: Int. J. Pure Appl. Anal. Chem. 67 (4), 43–47.
Goyal, S.K., Seyfried, M.S., O'Neill, P.E., 1999. Correction of surface roughness and topographic effects on airborne SAR in mountainous rangeland areas. Remote Sens. Environ. 67 (2), 124–136.
Heathman, G.C., Cosh, M.H., Merwade, V., Han, E., 2012. Multi-scale temporal stability analysis of surface and subsurface soil moisture within the Upper Cedar Creek Watershed, Indiana. Catena. 95, 91–103.
Holzman, M.E., Carmona, F., Rivas, R., Niclos, R., 2018. Early assessment of crop yield from remotely sensed water stress and solar radiation data. Isprs J. Photogramm. Remote Sens. (Basel) 145PB, 297–308.
Jacquemoud, S., Baret, F., Hanocq, J.F., 1992. Modeling spectral and directional soil reflectance. Remote Sens. Environ. 41 (2), 123–132.
Kang, S., Hao, X., Du, T., Tong, L., Su, X., Lu, H., Li, X., Huo, Z., Li, S., Ding, R., 2016. Improving agricultural water productivity to ensure food security in China under changing environment: From research to practice. Agric. Water Manag. 179, 5–17.
Kara, A., Pekel, E., Ozcetin, E., Yldz, G.B., 2024. Genetic algorithm optimized a deep learning method with attention mechanism for soil moisture prediction. Neural Comput. Applic. 36 (4), 1761–1772.
Kerr, Y.H., Waldteufel, P., Richaume, P., Wigneron, J.P., Ferrazzoli, P., Mahmoodi, A., Al Bitar, A., Cabot, F., Gruhier, C., Juglea, S.E., 2012. The SMOS soil moisture retrieval algorithm. IEEE Trans. Geosci. Remote Sens. 50, 1384–1403.
Knadel, M., Rossel, R.A.V., Deng, F., Thomsen, A., Greve, M.H., 2013. Visible-near infrared spectra as a proxy for topsoil texture and glacial boundaries. Soil Sci. Soc. Am. J. 77 (2), 568–579.
Kubelka, P., Munk, F., 1931. Ein Beitrag zur Optik der Farbanstriche (Contribution to the optic of paint). Zeitschrift Fur Technische Physik. 12, 593–601.
Kumar, S.V., Dirmeyer, P.A., Peters-Lidard, C.D., Bindlish, R., Bolten, J., 2018. Information theoretic evaluation of satellite soil moisture retrievals. Remote Sens. Environ. 204, 392–400.
Lobell, D.B., Asner, G.P., 2002. Moisture Effects on Soil Reflectance. Soil Sci. Soc. Am. J. 66 (3), 722–727.
Morellos, A., Pantazi, X.-E., Moshou, D., Alexandridis, T., Whetton, R., Tziotzios, G., Wiebensohn, J., Bill, R., Mouazen, A.M., 2016. Machine learning based prediction of soil total nitrogen, organic carbon and moisture content by using VIS-NIR spectroscopy. Biosyst. Eng. 152, 104–116.
Ou, D., Tan, K., Wang, X., Wu, Z., Li, J., Ding, J., 2022. Modified soil scattering coefficients for organic matter inversion based on Kubelka-Munk theory. Geoderma. 418, 115845.
Patel, N.R., Anapashsha, R., Kumar, S., Saha, S.K., Dadhwal, V.K., 2009. Assessing potential of modis derived temperature/vegetation condition index (TVDI) to infer soil moisture status. Int. J. Remote Sens. 30 (1–2), 23–39.
Polak, A., Wallach, R., 2001. Analysis of soil moisture variations in an irrigated orchard root zone. Plant & Soil. 233 (2), 145–159.
Roosjen, P., Bartholomeus, H., Clevers, J., 2015. Effects of soil moisture content on reflectance anisotropy—Laboratory goniometer measurements and RPV model inversions. Remote Sens. Environ. 170, 229–238.
Sadeghi, M., Babaeian, E., Tuller, M., Jones, S.B., 2017. The optical trapezoid model: a novel approach to remote sensing of soil moisture applied to Sentinel-2 and Landsat-8 observations. Remote Sens. Environ. 198, 52–68.
Sadeghi, M., Jones, S.B., Philpot, W.D., 2015. A linear physically-based model for remote sensing of soil moisture using short wave infrared bands. Remote Sens. Environ. 164, 66–76.
Shen, X., Walker, J.P., Ye, N., Wu, X., Nithyapriya, B., Yeo, I.Y., 2021. Soil moisture retrieval depth of P- and L-band radiometry: predictions and observations. IEEE Trans. Geosci. Remote Sens. 59 (8), 6814–6822.
Schmidinger, J., Heuvelink, G.B.M., 2023. Validation of uncertainty predictions in digital soil mapping. Geoderma. 437, 116585.
Suyoung, P., Dongryeol, R., Sigfredo, F., Hoam, C., Esther, H.-M., Mark, O.C., 2017. Adaptive estimation of crop water stress in nectarine and peach orchards using high-resolution imagery from an unmanned aerial vehicle (UAV). Remote Sens. (Basel). 9 (8), 1–15.
Tan, K., Chen, L., Wang, H., Liu, Z., Ding, J., Wang, X., 2023. Estimation of the distribution patterns of heavy metal in soil from airborne hyperspectral imagery based on spectral absorption characteristics. J. Environ. Manage. 347, 119196.
Vargas, W.E., G. A, N., 1997. Applicability conditions of the Kubelka-Munk theory. Appl. Opt. 36 (22), 5580–5586.
Viscarra Rossel, R.A., Behrens, T., 2010. Using data mining to model and interpret soil diffuse reflectance spectra. Geoderma. 158 (1–2), 46–54.
Wang, C., Wu, X.H., Li, L.Q., Wang, Y.S., Li, Z.W., 2018. Convolutional neural network application in prediction of soil moisture content. Spectroscopy Spectral Anal. 38, 36–41.
Wang, J., Wu, Y., Zhang, Y., Wang, H., Yan, H., Jin, H., 2024. A genetic algorithm-optimized backpropagation neural network model for predicting soil moisture content using spectral data. J. Soil. Sediment. 24 (7), 2816–2828.

Wu, F., Tan, K., Wang, X., Ding, J., Liu, Z., Han, B., 2023. A semi-analytical radiative transfer model for explaining soil spectral features. Int. J. Appl. Earth Obs. Geoinf. 118, 103250.
Yang, G.J., Zhao, C.J., Huang, W.J., Wang, J.H., 2011. Extension of the Hapke bidirectional reflectance model to retrieve soil water content. Hydrol. Earth Syst. Sci. Discuss. 15 (7), 2317–2326.
Yang, Y., Shang, S., Jiang, L.J.A., 2012. Remote sensing temporal and spatial patterns of evapotranspiration and the responses to water management in a large irrigation district of North China. Agric. Forest Meteorol. 164, 112–122.
Yao, P., Lu, H., Shi, J., Zhao, T., Yang, K., Cosh, M.H., Gianotti, D.J.S., Entekhabi, D., 2021. A long term global daily soil moisture dataset derived from AMSR-E and AMSR2 (2002-2019). Sci Data. 8, 143.
Yuan, J., Wang, X., Yan, C.X., Wang, S.R., Ju, X.P., Li, Y., 2019. Soil Moisture retrieval model for remote sensing using reflected hyperspectral information. Remote Sens. (Basel). 11 (3), 1–17.
Yue, J., Tian, J., Tian, Q., Xu, K., Xu, N., 2019. Development of soil moisture indices from differences in water absorption between shortwave-infrared bands. ISPRS J. Photogramm. Remote Sens. 154, 216–230.
Zhang, Y., Tan, K., Wang, X., Chen, Y., 2020. Retrieval of soil moisture content based on a modified Hapke photometric model: a novel method applied to laboratory hyperspectral and sentinel-2 MSI data. Remote Sens. (Basel). 12 (14), 1–21.